Histol Histopathol (2024) 39: 493-508

Histology and Histopathology
From Cell Biology to Tissue Engineering

ORIGINAL ARTICLE Open Access

Expression pattern, immune signature, and prognostic value of RBM10 in human cancers

Xi Sun, Dexin Jia and Yan Yu

Department of Medical Oncology, Harbin Medical University Cancer Hospital, Harbin, China

Summary. Background. RNA-binding motif protein 10 (RBM10) regulates the expression of genes involved in immune responses and is associated with a wide spectrum of cancers. Meanwhile, immunotherapy is the most promising cancer treatment of our time; nevertheless, the pan-cancer role of RBM10 remains to be elucidated.

Methods. Data from multiple online databases, including ONCOMINE, UALCAN, GEPIA2, Kaplan–Meier Plotter, cBioPortal, STRING, and TIMER were analyzed. The protein expression levels of RBM10 in various tumor types were verified by immunohistochemistry (IHC).

Results. RBM10 is upregulated in multiple tumors compared with the corresponding normal tissues. In addition, RBM10 is highly mutated in various cancers. We also compared the levels of phosphorylated RBM10 between normal and primary tumor tissues. We found that the expression of RBM10 was positively correlated with Programmed cell death 1 (PD-L1) and Cytotoxic lymphocyte antigen 4 (CTLA4) in most cancers, except Thyroid carcinoma (THCA). Moreover, the expression of RBM10 was significantly related to immune cell infiltration in many cancers, suggesting that it is a promising target for cancer immunotherapy.

Conclusions. RBM10 expression is closely related to tumor prognosis and the immune microenvironment. Our findings provide new insights into the role of RBM10 in cancer diagnosis and treatment.

Key words: RBM10, Pan-cancer, Survival analysis, Immune microenvironment

Introduction

Radiotherapy, chemotherapy, and immunotherapy are currently the most common treatment strategies for cancer. Multiple studies have shown that compared with chemotherapy, PD-1/PD-L1 inhibitors can significantly improve the outcomes of cancer patients (Yuan et al., 2023; Zheng et al., 2023; Zhu et al., 2023). However, many patients fail to respond to immunotherapy or have drug resistance (Benci et al., 2016; Murciano-Goroff et al., 2020). Thus, it is crucial to elucidate the molecular mechanisms underlying tumor progression in order to identify immune-related genes of prognostic and therapeutic relevance.

RNA binding proteins (RBPs) play essential roles in RNA metabolism and post-transcriptional gene regulation (Okholm et al., 2020; Mushtaq et al., 2023; Yin et al., 2023). RNA-binding motif protein 10 (RBM10), also known as S1–1, consists of two RNA recognition motif (RRM) domains, an OCRE domain, a G-patch domain, a C2H2-type zinc finger domain, a RanBP2-type zinc finger domain, and three nuclear localization signals (NLSs) (Johnston et al., 2010; Xiao et al., 2013). RBM10 has multiple alternative splice variants and isoform expression profiles (Inoue et al., 2014). Isoform 1 (RBM10v1) is the predominantly expressed form, therefore, it is the most extensively studied RBM10 isoform. (Bechara et al., 2013; Wang et al., 2013). It is ubiquitously expressed, more strongly so in cells with active transcription (Loiselle et al., 2017; Rodor et al., 2017; Sun et al., 2019).

Several studies have shown that RBM10 expression is correlated with mRNA stabilization (Mueller et al., 2009), alternative splicing (Bechara et al., 2013; Wang et al., 2013; Zheng et al., 2013; Inoue et al., 2014),

Corresponding Author: Xi Sun, Department of Medical Oncology, Harbin Medical University Cancer Hospital, Harbin, China. e-mail: canghaochibang@163.com

www.hh.um.es. DOI: 10.14670/HH-18-790

Abbreviations. BLCA, Bladder Urothelial carcinoma; BRCA, Breast invasive carcinoma; CHOL, Cholangiocarcinoma; COAD, Colon adenocarcinoma; ESCA, Esophageal carcinoma; HNSC, Head and Neck squamous cell carcinoma; LIHC, Liver hepatocellular carcinoma; LUAD, Lung Adenocarcinoma; LUSC, Lung squamous cell carcinoma; PRAD, Prostate Adenocarcinoma; READ, Rectum adenocarcinoma; STAD, Stomach adenocarcinoma; KIRC, Kidney Renal Clear Cell carcinoma; THCA, Thyroid carcinoma; UCEC, Uterine Corpus Endometrial carcinoma; DLBC, Diffuse large B-cell lymphoma; SARC, Sarcoma; THYM, Thymoma; ACC, Adrenocortical carcinoma; KICH, Kidney chromophobe; PAAD, pancreatic adenocarcinoma; SKCM, Skin Cutaneous Melanoma; KIRP, Kidney renal papillary cell; OV, Ovarian serous cystadenocarcinoma; IHC, immunohistochemistry.

translation (Zhang et al., 2020b), immune activity (Liu et al., 2021b), apoptosis (Jung et al., 2020a,b), cell cycle arrest (Pang et al., 2022), cell proliferation (Bechara et al., 2013; Jin et al., 2019; Wu et al., 2022), and anti-viral responses (Pozzi et al., 2020). RBM10's cellular functions are beginning to be explored, with initial studies demonstrating a tumor suppressor role. Very recently, however, contradictory results have emerged, suggesting a tumor promoter role for RBM10. Moreover, the role of RBM10 has been evaluated in only a few cancers, and its pan-cancer expression levels, immunological function, and prognostic value remain underexplored.

In this study, we analyzed the pan-cancer expression pattern, immune signature, and prognostic value of RBM10 using genomic, transcriptomic, clinical, and pathway data retrieved from public databases. The expression levels of RBM10 across different tumor types were also validated by immunohistochemistry (IHC). Our findings provide new insights into the roles of RBM10 in cancer and immunotherapy.

Materials and methods

Gene expression analysis

We used TIMER2 (tumor immune estimation resource, version 2, http://timer.cistrome.org/) to seek the expression of RBM10 in the tumor and adjacent normal tissues. However, some cancers showed no normal tissue, (e.g., The Cancer Genome Atlas (TCGA)-Adrenocortical Carcinoma (ACC), TCGA-Cervical squamous cell carcinoma and endocervical adenocarcinoma (CESC), we applied the GEPIA2 (Gene Expression Profiling Interactive Analysis, version 2) tool (http://gepia2.cancer-pku.cn/#analysis) to obtain box plots of the GTEx (Genotype-Tissue Expression) database, setting a *p*-value cut-off = 0.01, log2FC (fold change) cut-off = 1, and "Match TCGA normal and GTEx data". We used the CPTAC (Clinical Proteomic Tumor Analysis Consortium) dataset to analyze expression levels of total protein or phosphoprotein of RBM10, compared between primary and normal tissues (Chen et al., 2019). The ONCOMINE database was utilized to analyze the transcription levels of RBM10 between disparate cancer tissues and their corresponding adjacent normal control samples (Rhodes et al., 2004). A p-value of 0.05, a fold change of 2, and a gene rank in the top 10% were set as the significance thresholds. Moreover, we obtained violin plots of RBM10 expression in different pathological stages (stage I-IV) of all TCGA tumors via the GEPIA2 tool.

Immunohistochemistry (IHC) staining

A human tissue microarray (TMA) containing a total of 51 pairs of tumor and matched adjacent normal tissues from 20 types of cancer including lung adenocarcinoma (LUAD), lung squamous cell carcinoma (LUSC), kidney renal clear cell carcinoma (KIRC), breast invasive carcinoma (BRCA), thyroid carcinoma (THCA), esophageal carcinoma (ESCA), stomach adenocarcinoma (STAD), colon adenocarcinoma (COAD), rectum adenocarcinoma (READ), pancreatic adenocarcinoma (PAAD), and Liver hepatocellular carcinoma (LIHC) was purchased from the Shanghai Outdo Biotech Company to evaluate differences in RBM10 expression at the protein level. Briefly, the microarray was stained with RBM10 (TA329114, Origene, 1:200) overnight at 4ºC. The secondary antibody was added and incubated at room temperature for 120 min according to the manufacturer's protocol. IHC images of RBM10 protein expression in normal tissues and six tumor tissues, including THCA, BRCA, COAD, ESCA, LIHC, and STAD were analyzed. Eventually, two independent investigators assessed RBM10 immunostaining. The percentage of protein-positive cells was calculated as follows: 0, (0%); 1, (1~25%); 2, (26~50%); 3, (51~75%); and 4, (76~100%). The intensity score was assigned a value of 0 (negative), 1 (weak), 2 (medium), and 3 (strong). The final staining score was calculated by adding the positive cell score and the intensity score (0-7). Immunocytochemistry (ICC) images were downloaded from the Human Protein Atlas (HPA) (http://www.proteinatlas.org/) to detect and visualize RBM10 protein in the human A431 epidermoid carcinoma cell line and the U-2OS osteosarcoma cell line using antibodies specific to the target.

Survival prognosis analysis

In this study, the Kaplan Meier plotter was used to evaluate the prognostic value of RBM10 mRNA expression, where cancer patients were split into high and low-expression groups. This was based on median values of mRNA expression and validated by K-M survival curves, with the hazard ratio (HR) with 95% confidence intervals (CI) and log-rank *p*-value (Nagy et al., 2018). A statistically significant difference was considered when a *p*-value was <0.05. Thereafter, we used GEPIA2 to obtain the disease-free survival (DFS) significance map data of RBM10 across all TCGA tumors. High and low expressions were divided by a 50% cutoff value. The hypothesis test adopted the log-rank test and the survival plots were received from the "Survival Analysis" module of GEPIA2 (Cui et al., 2020).

Genetic alteration analysis

We used the cBioPortal tool (https://www.cbioportal.org/) to collect the data on alteration frequency, mutation type, mutated site information, Copy number alteration (CNA), and Three dimensional (3D) structure of the protein across all TCGA tumors (Gao et al., 2013). Survival data, including Overall survival (OS), Progression-free survival (PFS), DFS, and Disease-specific survival (DSS) were compared for Bladder

Urothelial carcinoma (BLCA), LUAD, and LUSC patients, with or without an RBM10 genetic alteration.

Immune infiltration analysis

The TIMER2 tool was used to analyze the relationship between RBM10 expression and PD-L1, CTLA4. We also utilized it to analyze the relationship between the expression of RBM10 and immune infiltrates. The EPIC, MCPCOUNTER, XCELL, and TIDE algorithms were applied for estimations (Sturm et al., 2019).

RBM10-related gene enrichment analysis

Herein, the online STRING database (https://cn.string-db.org/) was applied to analyze associations among the protein-protein interaction network of RBM10, the species was set to *Homo sapiens*, minimum required interaction score ["Low confidence (0.150)"], max number of interactors to show ("no more than 50 interactors" in 1st shell), meaning of network edges ("evidence"), and active interaction sources ("experiments").

We obtained the top 100 genes associated with RBM10 through the GEPIA2 website. We then conducted a paired gene-gene Pearson correlation analysis between RBM10 and the selected genes. *p*-values and correlation coefficients (R values) were calculated and indicated in the corresponding figure panels. The heatmap representation of the expression profile for the selected genes contains the partial correlation (cor) and *p*-value in the purity-adjusted Spearman's rank correlation test. The Kyoto Encyclopedia of Genes and Genomes (KEGG) and gene ontology (GO) analyses were performed using the genes associated or interacting with RBM10. The R language software [R-3.6.3, 64-bit] (https://www.r-project.org/) was used in this analysis. $p<0.05$ was considered statistically significant (Yu et al., 2012).

Results

RBM10 is aberrantly expressed in different cancer types

The differential expression of RBM10 between tumors and adjacent normal tissues in TCGA was analyzed using TIMER2. As shown in Figure 1A, RBM10 was upregulated in BLCA, BRCA, cholangiocarcinoma (CHOL), COAD, ESCA, head and neck squamous cell carcinoma (HNSC), LIHC, LUAD, LUSC, PRAD, READ, and STAD compared with the corresponding control tissues, whereas other tumor types such as KIRC, THCA, and uterine Corpus Endometrial carcinoma (UCEC) showed no differential expression pattern. Further analysis using the GTEx dataset revealed that CHOL, diffuse large B-cell lymphoma (DLBC), sarcoma (SARC), and THYM expressed higher levels of RBM10 compared with their normal counterparts (Fig. 1B). On the other hand, there was no significant difference for ACC, BLCA, BRCA, LUAD, or LUSC. The differential expression of the RBM10 protein was analyzed using the CPTAC dataset of the National Cancer Institute. As shown in Figure 1C, the

Table 1. Correlation between RBM10 expression and immune cells.

Immune cells	Cancer types	Rho	*p*-value
CD8+ T	ACC (n=79)	0.21	0.07
	BLCA (n=408)	0.20	<0.001
	BRCA (n=1100)	0.10	0.001
	HNSC (n=522)	0.36	1.25E-16
	LIHC (n=371)	0.25	1.63E-06
	STAD (n=415)	0.17	0.001
	THCA (n=509)	<-0.01	0.98
	OV (n=303)	0.12	0.06
	PRAD (n=498)	0.17	<0.001
	LUAD (n=515)	0.04	0.35
CD4+ T	ACC (n=79)	0.15	0.21
	BLCA (n=408)	0.05	0.36
	BRCA (n=1100)	0.21	2.97E-11
	HNSC (n=522)	0.45	1.38E-25
	LIHC (n=371)	0.36	6.03E-12
	STAD (n=415)	0.23	5.82E-06
	THCA (n=509)	-0.06	0.21
	OV (n=303)	0.14	0.03
	PRAD (n=498)	0.11	0.03
	LUAD (n=515)	0.23	1.96E-07
B	ACC (n=79)	-0.03	0.80
	BLCA (n=408)	0.12	0.02
	BRCA (n=1100)	0.11	<0.001
	HNSC (n=522)	-0.30	7.47E-12
	LIHC (n=371)	0.44	1.22E-17
	STAD (n=415)	0.06	0.25
	THCA (n=509)	0.14	0.003
	OV (n=303)	-0.01	0.93
	PRAD (n=498)	0.12	0.011
	LUAD (n=515)	0.10	0.02
Macrophage	ACC (n=79)	0.05	0.65
	BLCA (n=408)	0.08	0.11
	BRCA (n=1100)	-0.16	8.43E-07
	HNSC (n=522)	-0.02	0.63
	LIHC (n=371)	0.39	7.29E-14
	STAD (n=415)	-0.05	0.34
	THCA (n=509)	0.26	5.88E-09
	OV (n=303)	0.36	5.44E-09
	PRAD (n=498)	0.16	<0.001
	LUAD (n=515)	-0.01	0.87
Neutrophil	ACC (n=79)	0.37	0.001
	BLCA (n=408)	0.10	0.07
	BRCA (n=1100)	0.16	8.55E-07
	HNSC (n=522)	0.04	0.42
	LIHC (n=371)	-0.05	0.37
	STAD (n=415)	0.27	1.53E-07
	THCA (n=509)	0.16	<0.001
	OV (n=303)	0.46	1.67E-14
	PRAD (n=498)	0.20	4.09E-05
	LUAD (n=515)	0.07	0.14
Dendritic	ACC (n=79)	0.19	0.11
	BLCA (n=408)	<-0.01	0.94
	BRCA (n=1100)	<-0.01	0.54
	HNSC (n=522)	0.23	2.87E-07
	LIHC (n=371)	0.36	3.24E-12
	STAD (n=415)	<-0.01	1.00
	THCA (n=509)	-0.31	5.00E-12
	OV (n=303)	0.05	0.41
	PRAD (n=498)	0.06	0.21
	LUAD (n=515)	-0.16	<0.001

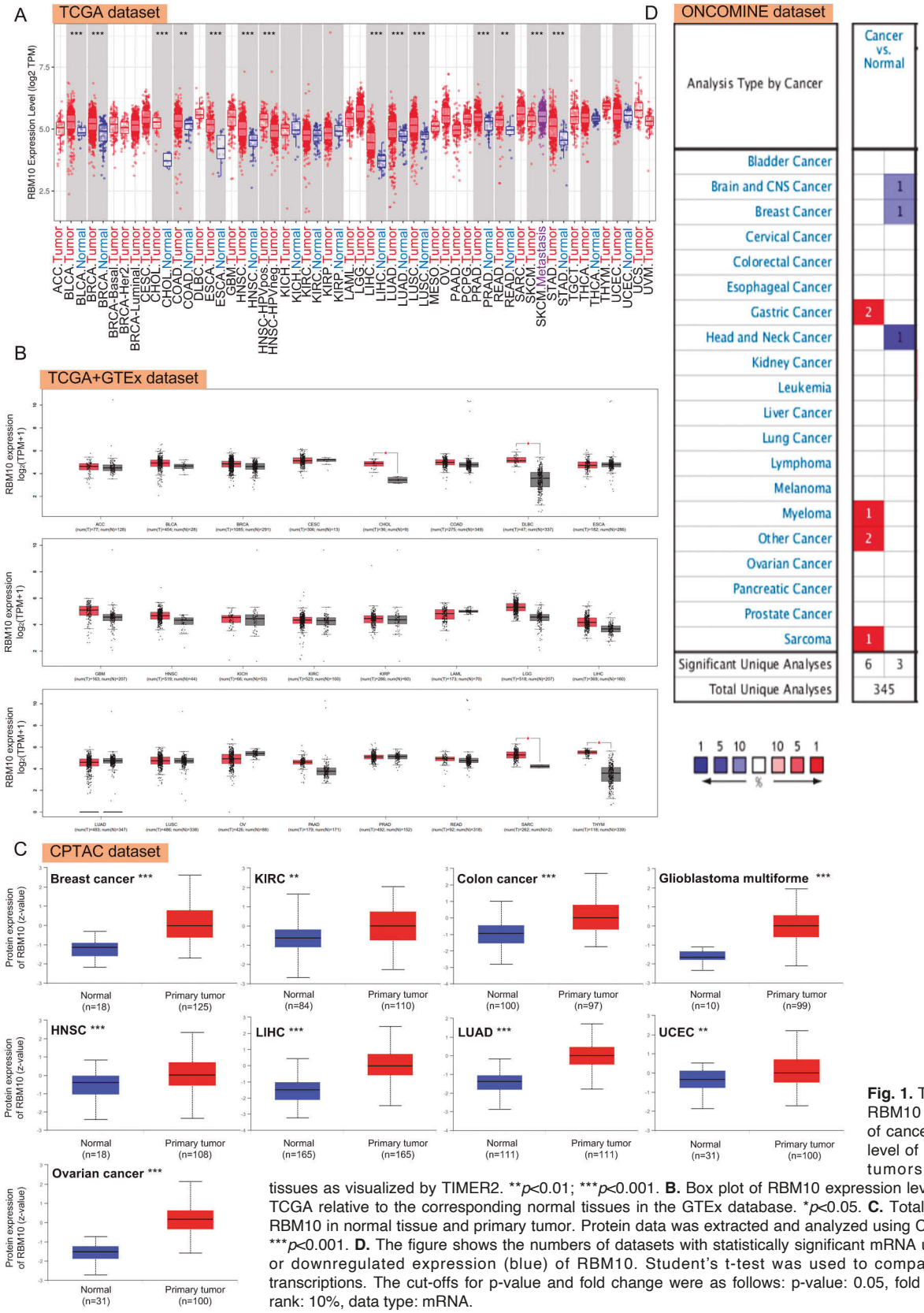

Fig. 1. The expression of RBM10 in distinct types of cancer. **A.** Expression level of RBM10 in TCGA tumors vs. normal tissues as visualized by TIMER2. **p<0.01; ***p<0.001. **B.** Box plot of RBM10 expression level comparison in TCGA relative to the corresponding normal tissues in the GTEx database. *p<0.05. **C.** Total protein levels of RBM10 in normal tissue and primary tumor. Protein data was extracted and analyzed using CPTAC. **p<0.01; ***p<0.001. **D.** The figure shows the numbers of datasets with statistically significant mRNA upregulated (red) or downregulated expression (blue) of RBM10. Student's t-test was used to compare the different transcriptions. The cut-offs for p-value and fold change were as follows: p-value: 0.05, fold change: 2, gene rank: 10%, data type: mRNA.

RBM10 protein level was significantly higher in KIRC, HNSC, LIHC, LUAD, UCEC, Ovarian serous cystadenocarcinoma (OV), breast cancer, colon cancer, and glioblastoma multiforme compared with normal tissues. In addition, RBM10 mRNA levels were markedly upregulated in gastric cancer tissues in the ONCOMINE database, as well as in other cancers from multiple datasets (Fig. 1D). Overall, RBM10 expression was elevated in most human tumors.

Furthermore, analysis using the GEPIA2 tool indicated that RBM10 expression was associated with tumor pathological staging in ACC, KICH, LIHC, OV, PAAD, and Skin Cutaneous Melanoma (SKCM) (Fig. 2), whereas no clear stage-specific expression changes were observed in other cancers.

To further confirm the dysregulation of RBM10 in cancer, we analyzed the paraffin-embedded tumor and peri-tumor tissues in the TMA. As shown in Figure 3A, normal thyroid, breast, colon, and stomach tissues were negative or moderately positive for RBM10, whereas tumor tissues had medium or strong staining. However, normal liver and esophageal tissues showed medium or strong staining for RBM10, while the corresponding tumor tissues were either negative or moderately positive. We compared these results with RBM10 expression data from TCGA and found that RBM10 expression levels in breast, colon, and stomach tissues were consistent with one another. The results for the other tissues were inconsistent, which can be attributed to the small sample size. The subcellular localization of

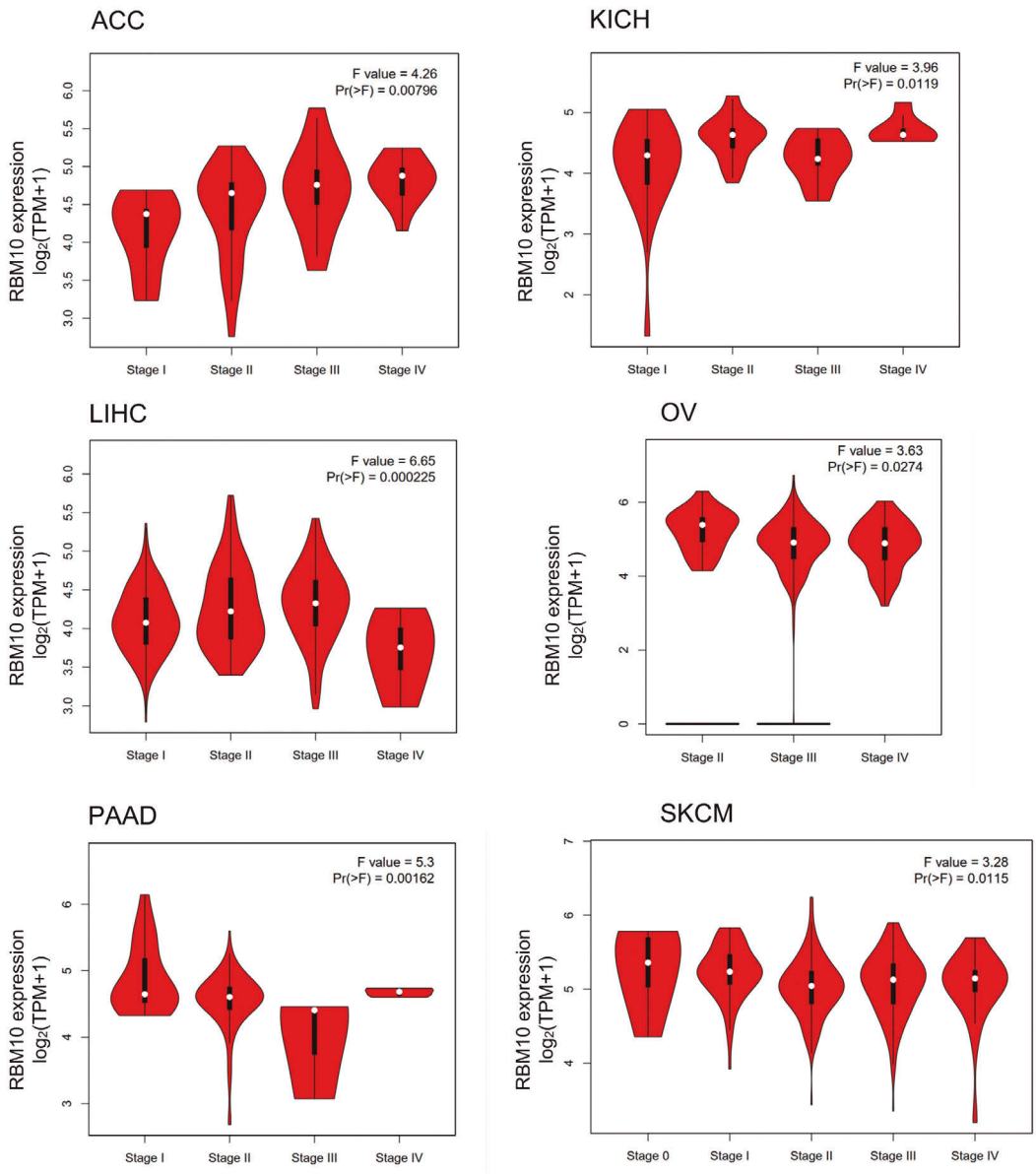

Fig. 2. Expression levels of RBM10 were analyzed in different pathological stages (stage I-IV) of ACC, KICH, LIHC, OV, PAAD, and SKCM. Log_2 (TPM + 1) was used to represent the expression levels.

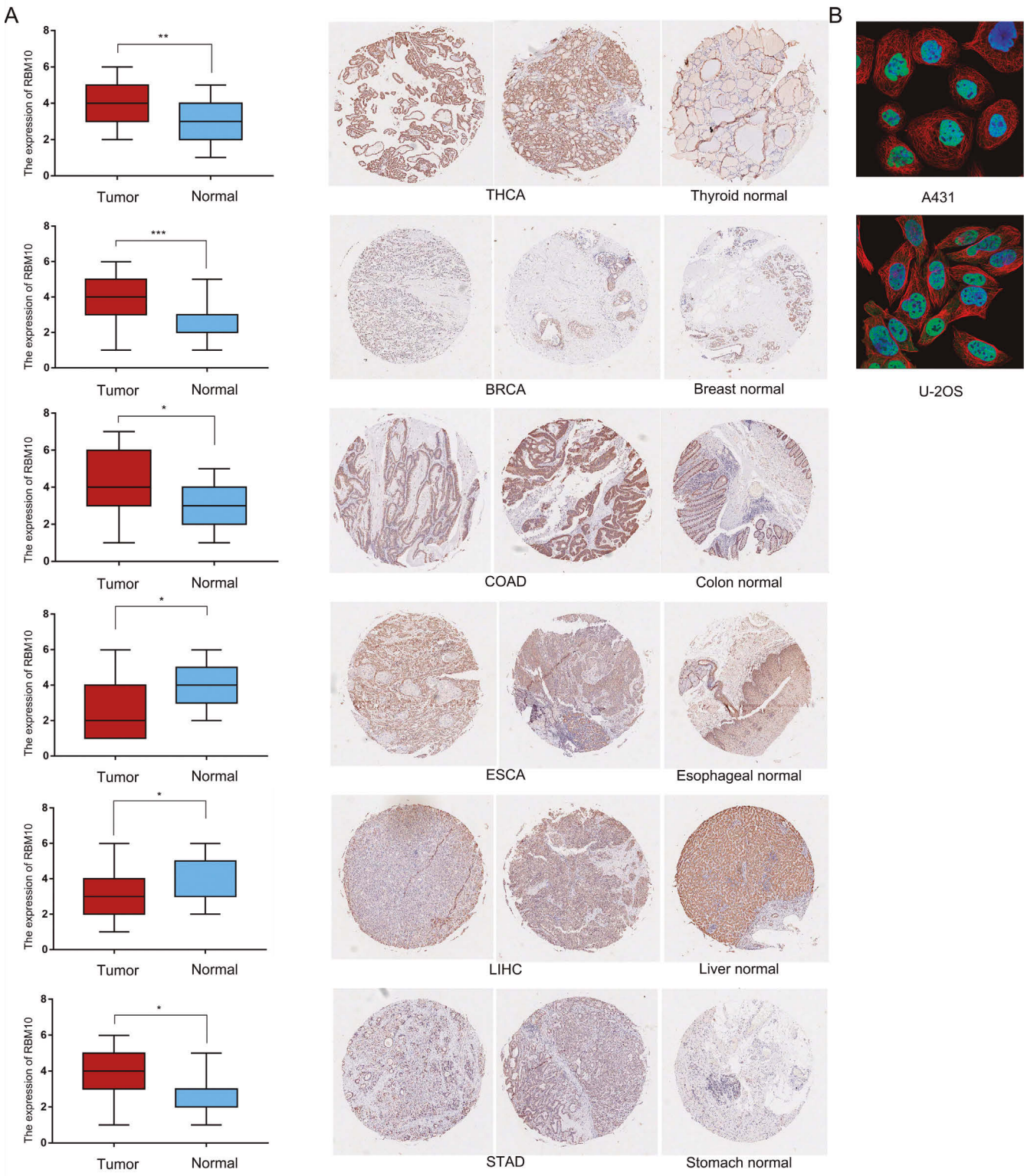

Fig. 3. Experimental verification of RBM10 expression. **A.** Comparison of RBM10 expression between tumor tissues and normal (left) and immunohistochemistry images in tumor (middle) and normal tissues (right). *p<0.05; **p<0.01; ***p<0.001. **B.** Immunocytochemistry for determining the subcellular location of RBM10 in A431 and U-2OS cell lines by HPA. RBM10 localized to the nucleus in blue (DAPI) and cytosol (green). Microtubules are stained in red.

the RBM10 protein in A431 and U-2OS cells was determined using ICC data from the HPA, and the results indicated that RBM10 was primarily expressed in the nuclear speckles and cytosol (Fig. 3B).

Association between RBM10 expression and survival

Analysis of the TCGA and GEO datasets revealed a significant correlation between RBM10 expression and patient prognosis including OS, Recurrence-free survival (RFS), and DFS. We divided the subjects into the $RBM10^{high}$ and $RBM10^{low}$ groups according to the RBM10 expression level. As shown in Figure 4A, high RBM10 expression indicated worse OS in KIRP and LIHC patients, whereas the opposite result was observed in PAAD patients. Furthermore, high RBM10 expression was associated with poor RFS in ESCA and LIHC, whereas its low expression portended poor RFS in STAD patients (Fig. 4B). We further analyzed the survival data using GEPIA2 and noted a correlation between high RBM10 expression levels and poor DFS for KIRP, LIHC, and PRAD (Fig. 4C).

Genetic variations of RBM10 and associations with cancer prognosis

Since genetic variation is a critical driver of tumor development, we next analyzed the mutation status of RBM10 in different tumors using cBioPortal. As shown in Figure 5B, the frequency of alterations in the *RBM10* gene sequence was the highest in bladder tumors (>10%), and "mutation" was the primary type. The different *RBM10* mutations and their sites are shown in Figure 5C. We did not detect any major genetic alteration and the locations were somewhat sporadic. For instance, the R153*/G alteration, in the PF14259 domain, was only detected in five cases. The location of R153*/G on the 3D structure of the RBM10 protein is shown in Figure 5A. We also analyzed the relationship between genetic alterations in *RBM10* and the prognosis of cancer patients and found that BLCA, LUAD, and LUSC patients harboring *RBM10* gene variations did not

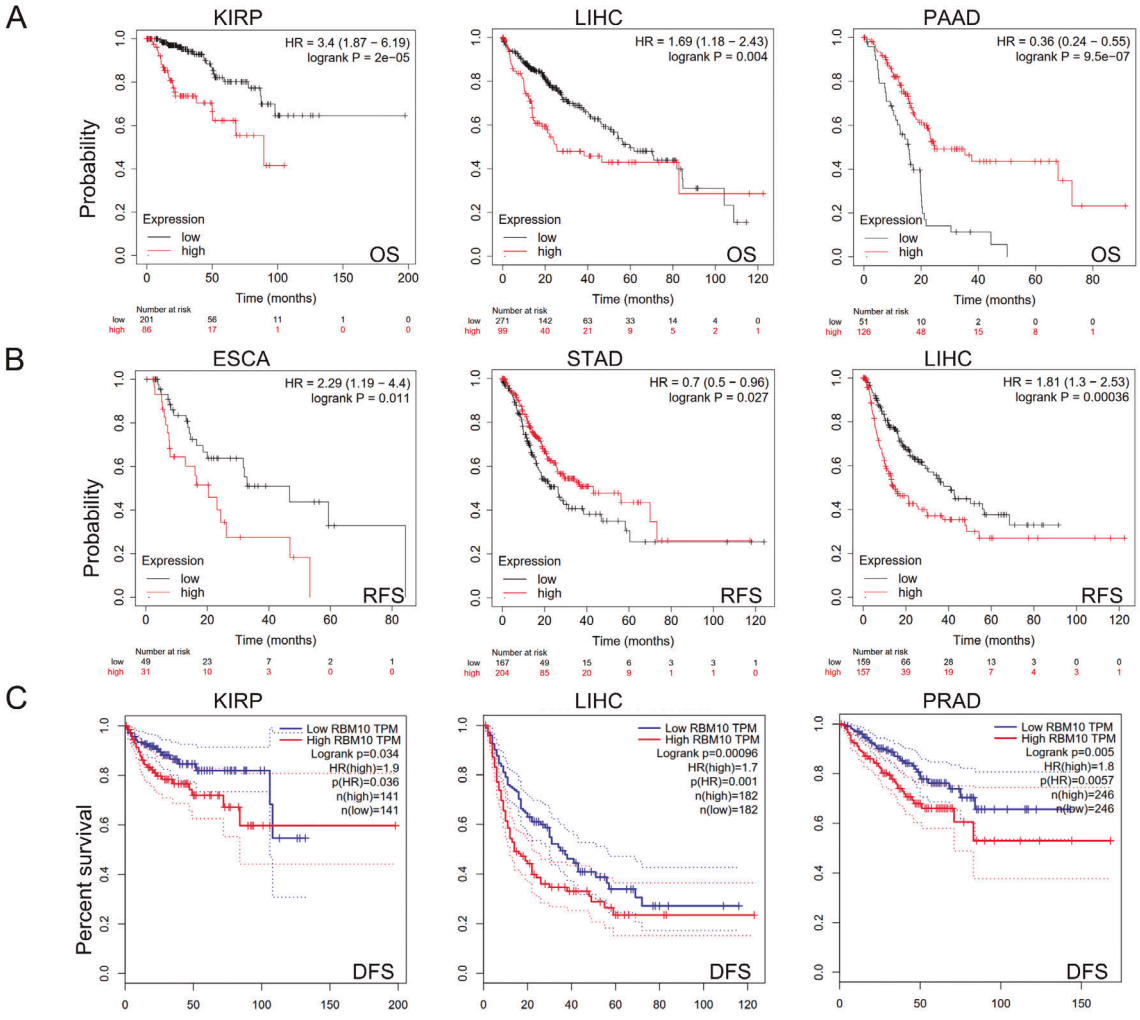

Fig. 4. Relationship between RBM10 expression levels and patient survival in TCGA tumors. **A.** Relationship between RBM10 expression and overall survival. **B.** Recurrence-free survival was assessed in all TCGA tumors using the Kaplan-Meier plotter database. **C.** Disease-free survival using GEPIA2. A *p*-value <0.05 is considered statistically significant, and only statistically significant results are shown here.

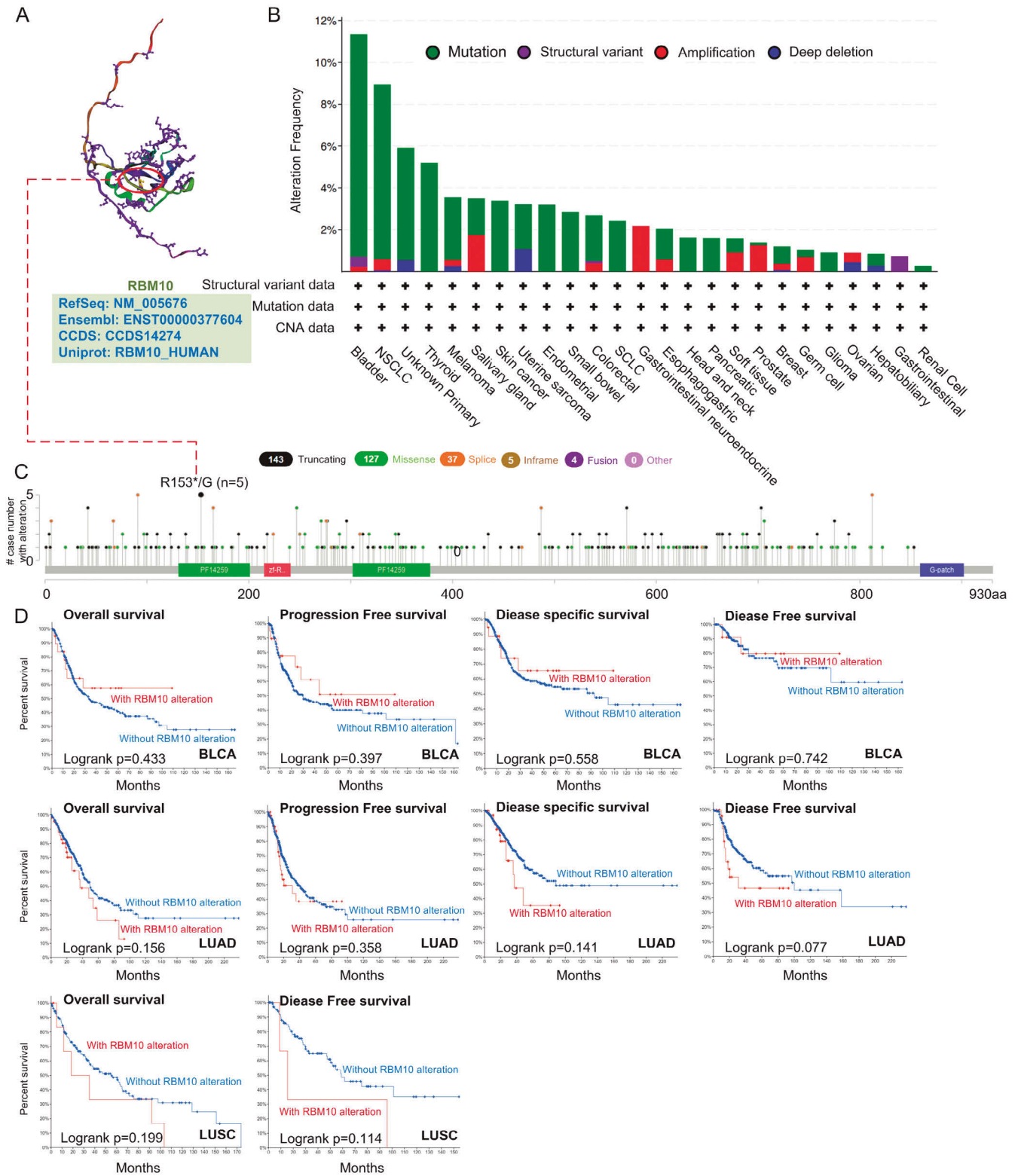

Fig. 5. Mutation status of *RBM10* in TCGA tumors. **A.** The mutation site (R153*/G) within the PF14259 domain is shown in the 3D structure of RBM10. **B.** The alteration frequency with mutation type **(C)** and mutation site are displayed. **D.** Analysis of the correlation between mutation status and OS, DSS, DFS, and PFS of BLCA, LUAD, and LUSC using the cBioPortal tool.

have better survival in terms of OS, PFS, DFS, and DSS, compared with patients without *RBM10* alterations (Fig. 5D).

Analysis data for RBM10 phosphorylation

There is ample evidence showing a correlation between aberrant protein phosphorylation and cancer progression (Kuang et al., 2016; Zhao et al., 2019; Liu et al., 2021a). Therefore, we also compared the phosphorylation of RBM10 between normal and primary tumor tissues in the CPTAC dataset. As shown in Figure 6A, the levels of phosphorylated RBM10S801 and RBM10S803 were significantly higher in primary LUAD and breast cancer tissues (Fig. 6B,C). Furthermore, there was increased phosphorylation of RBM10 at S30, T156, and S788 in breast cancer, and at T951, S910, and S862 in LUAD (Fig. 6B,C).

Association between RBM10 expression and immune checkpoints

Previous studies have shown that RBM10 is associated with the anti-tumor immune response (Liu et al., 2021b). We analyzed the correlation between the expression levels of RBM10 and that of the immune checkpoints PD-L1 and CTLA4 in diverse cancer types. As shown in Figure 7A, the expression of RBM10 was positively correlated with that of PD-L1 in ACC, BLCA, HNSC, STAD, LIHC, OV, and PRAD; it was negatively correlated with that of PD-L1 in THCA. No correlation was observed between the expression of RBM10 and PD-L1 in LUAD. In addition, RBM10 expression showed a positive correlation with that of CTLA4 in HNSC, STAD, LIHC, and LUAD, a negative correlation with that of CTLA4 in THCA, and no significant correlation with that of CTLA4 in the other four cancers (Fig. 7B).

Correlation between RBM10 expression and immune infiltration

Tumor-infiltrating immune cells participate in tumor genesis, progression, and metastasis (Zhang et al., 2020a; 2021; Mao et al., 2021; Xing et al., 2021). Furthermore, stromal cells in the tumor micro-environment, including cancer-associated fibroblasts (CAFs) and endothelial cells, regulate the functions of infiltrating immune cells (Chouaib et al., 2010, Mao et al., 2021; Soongsathitanon et al., 2021). Therefore, we examined the relationship between RBM10 expression and the infiltration of immune and stromal cells across different cancer types using TIMER. As shown in Table 1, RBM10 showed a significant positive correlation with the infiltration of CD8+ T cells, CD4+ T cells, B cells, and neutrophils, and a negative correlation with macrophages in BRCA. Similar trends were observed in PRAD, except that RBM10 was also positively correlated with the infiltration of macrophages. There was a positive correlation between the expression of RBM10 and infiltration of CD8+ T cells, CD4+ T, B cells, macrophages, and dendritic cells (DCs) in LIHC.

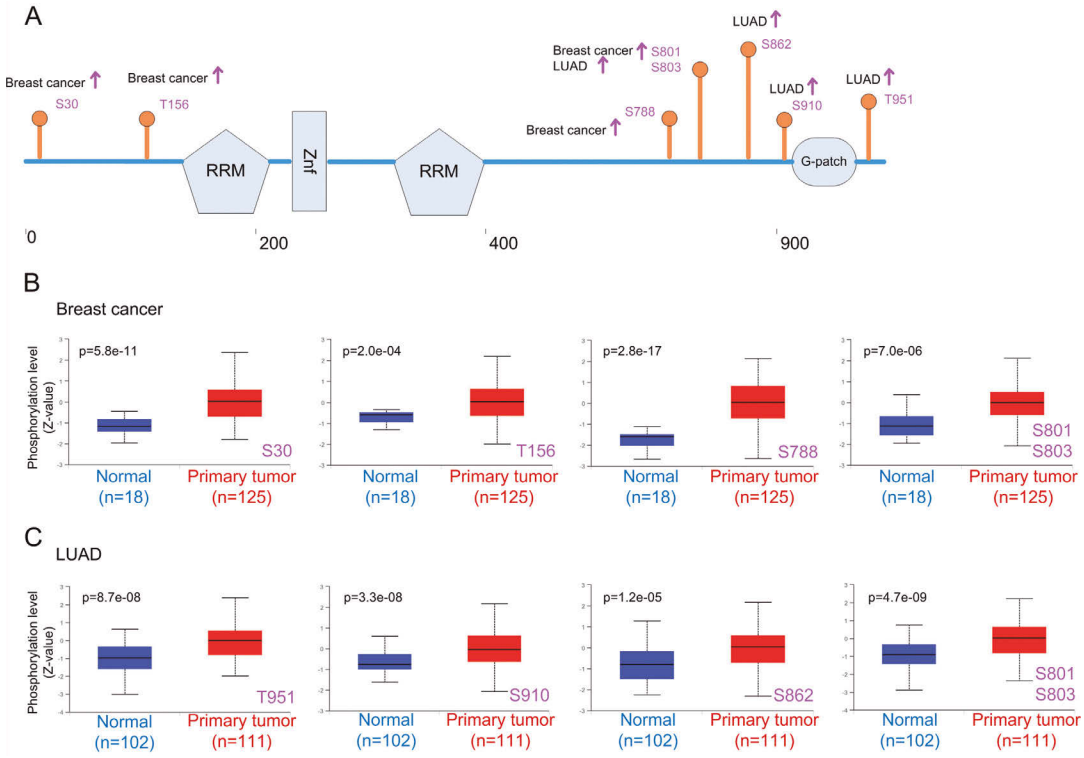

Fig. 6. Tumor-associated protein phosphorylation of RBM10. **A.** Phosphoprotein sites detected based on the CPTAC dataset in RBM10 are depicted in a schematic diagram. **B, C.** Box plot representation of RBM10 phosphoprotein levels in breast cancer and LUAD.

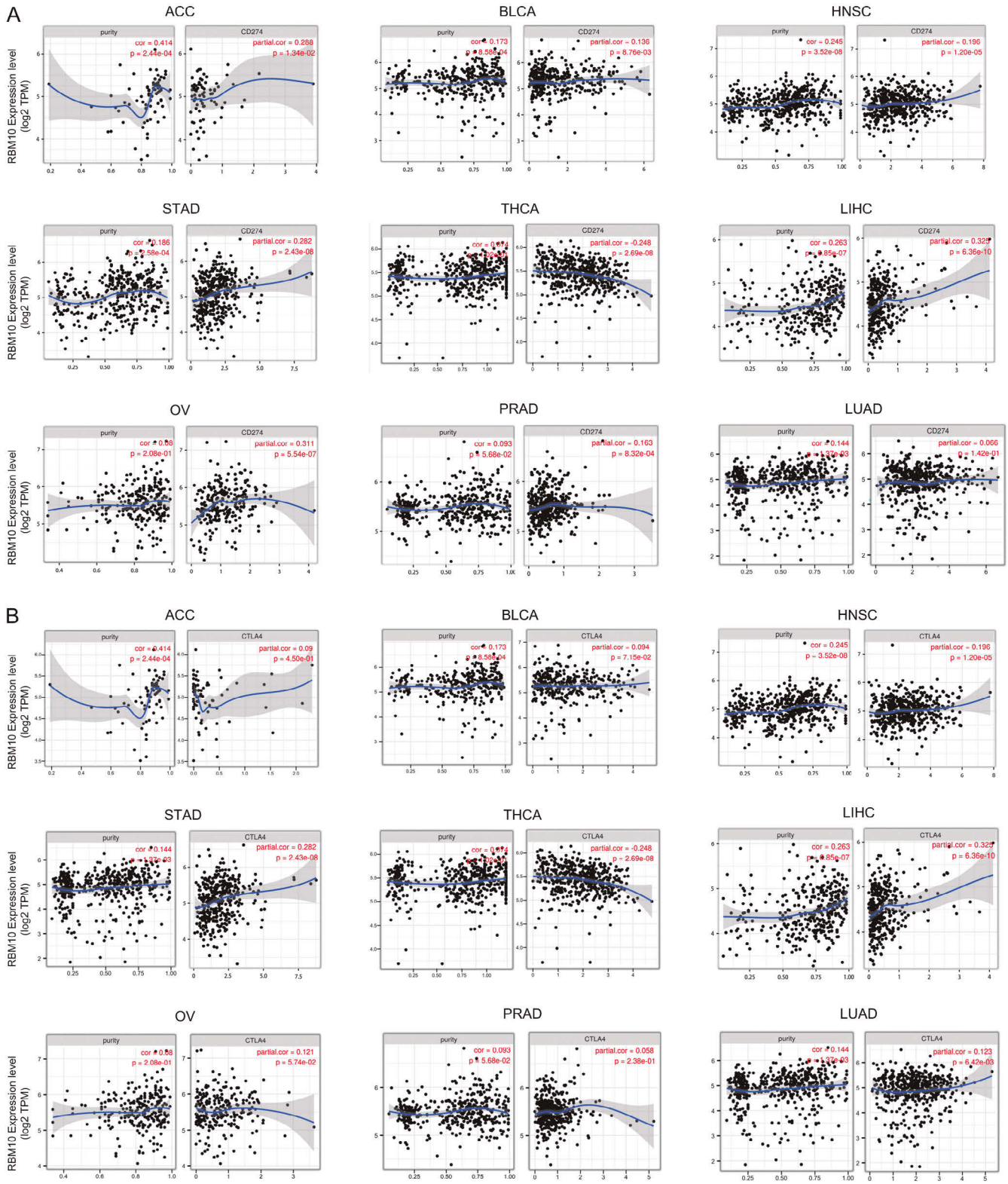

Fig. 7. The relationship between RBM10 and immune checkpoints. **A.** Correlations between RBM10 expression and PD-L1. **B.** Correlations between RBM10 expression and CTLA4 (TIMER). A *p*-value <0.05 is considered statistically significant.

In the HNSC samples, RBM10 expression was positively correlated with the infiltration of CD8+ T cells, CD4+ T cells, and DCs, and negatively correlated with that of B cells. RBM10 expression also showed a positive correlation with the infiltration of CD8+ T cells, CD4+ T cells, and neutrophils in STAD, and with CD4+ T cells, macrophages, and neutrophils in OV. Furthermore, RBM10 was positively correlated with the infiltration of B cells, macrophages, and neutrophils, and negatively correlated with that of DCs in THCA. We also observed a positive correlation of RBM10 expression with the infiltration of CD8+ T cells and B cells in BCLA and with that of CD4+ T cells and B cells in LUAD, while a negative correlation was seen with the infiltration of DCs in LUAD. In ACC, RBM10 expression was positively correlated with neutrophil

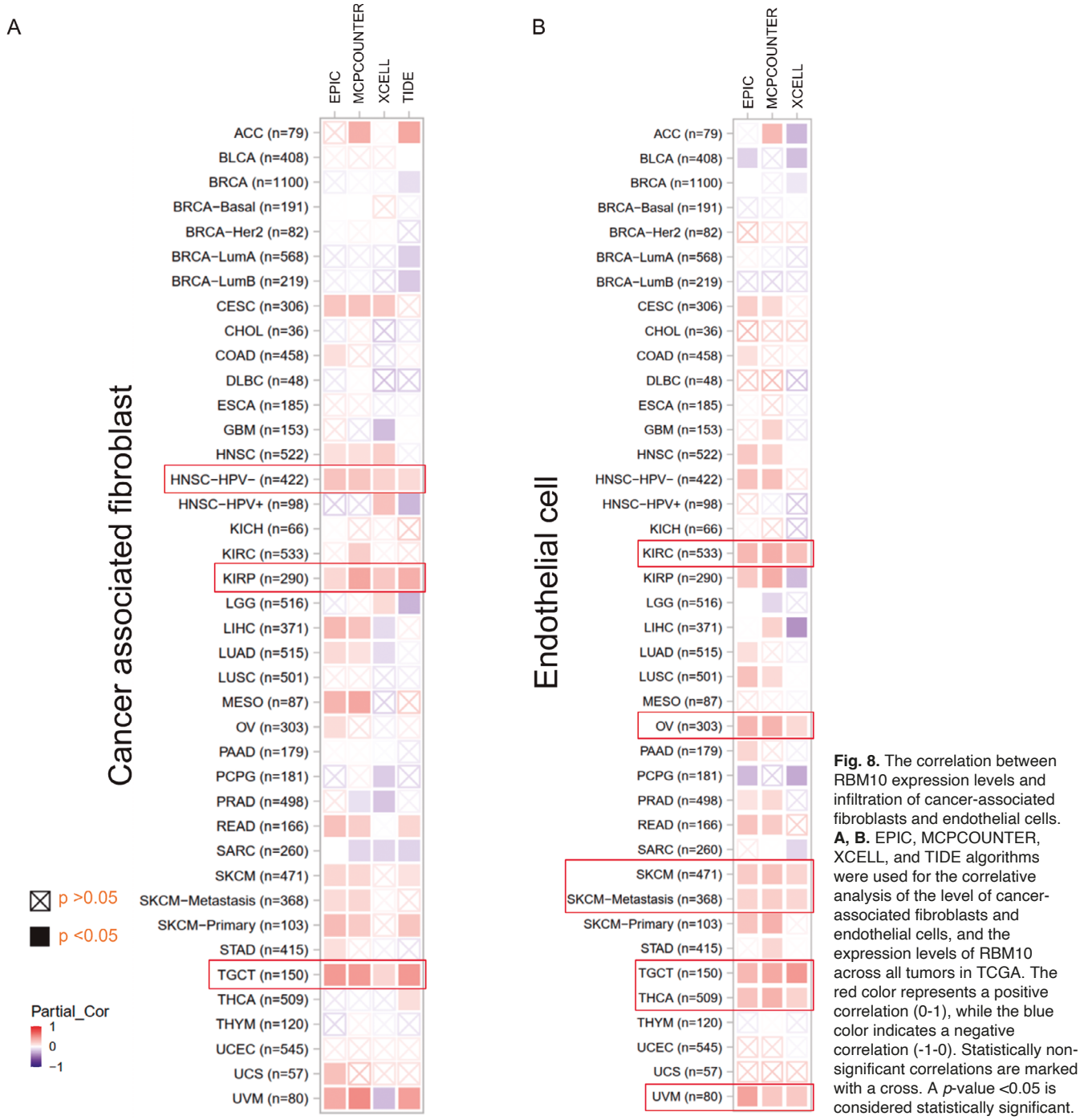

Fig. 8. The correlation between RBM10 expression levels and infiltration of cancer-associated fibroblasts and endothelial cells. **A, B.** EPIC, MCPCOUNTER, XCELL, and TIDE algorithms were used for the correlative analysis of the level of cancer-associated fibroblasts and endothelial cells, and the expression levels of RBM10 across all tumors in TCGA. The red color represents a positive correlation (0-1), while the blue color indicates a negative correlation (-1-0). Statistically non-significant correlations are marked with a cross. A *p*-value <0.05 is considered statistically significant.

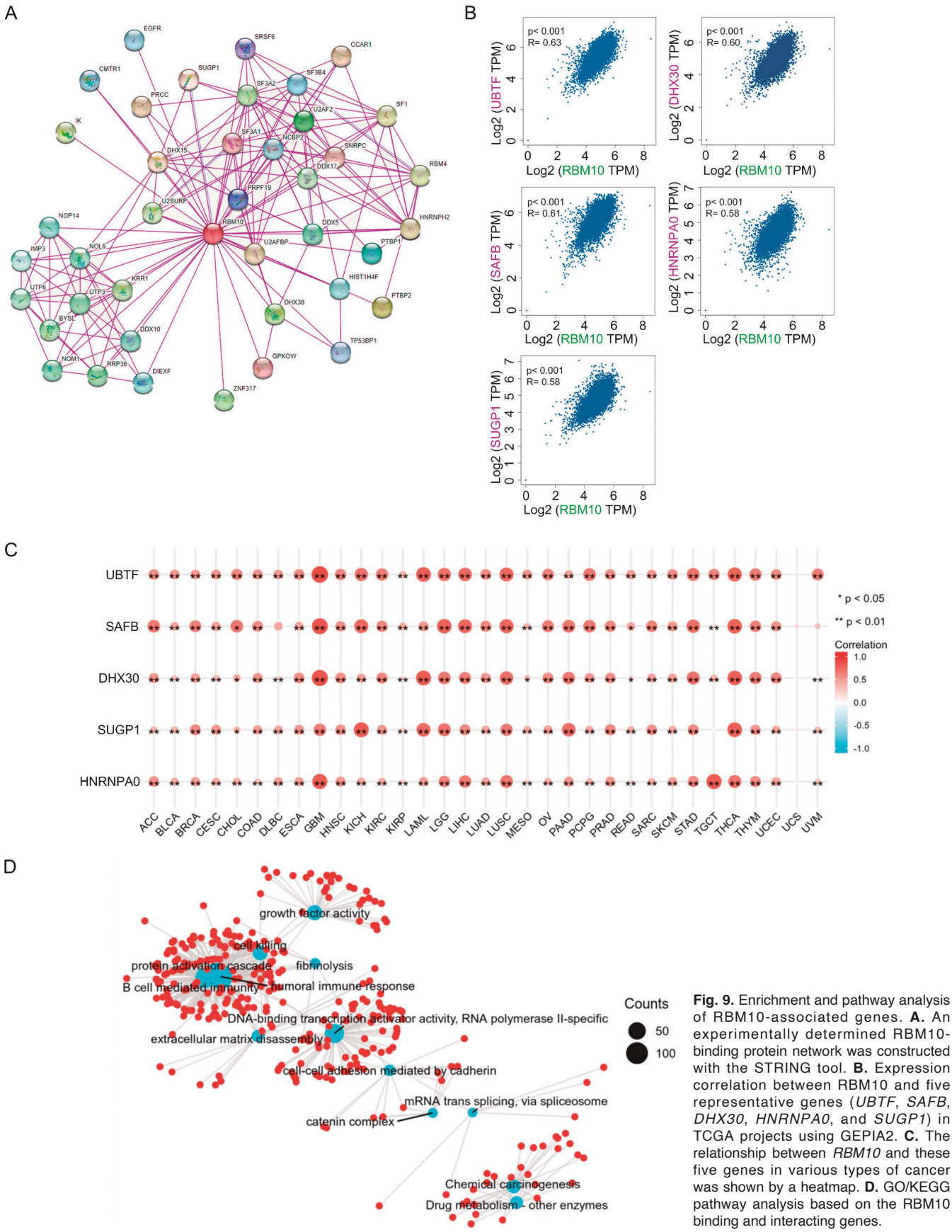

Fig. 9. Enrichment and pathway analysis of RBM10-associated genes. **A.** An experimentally determined RBM10-binding protein network was constructed with the STRING tool. **B.** Expression correlation between RBM10 and five representative genes (*UBTF*, *SAFB*, *DHX30*, *HNRNPA0*, and *SUGP1*) in TCGA projects using GEPIA2. **C.** The relationship between *RBM10* and these five genes in various types of cancer was shown by a heatmap. **D.** GO/KEGG pathway analysis based on the RBM10 binding and interacting genes.

infiltration.

The correlation between RBM10 expression and stromal cells in multiple tumor types was analyzed using the EPIC, MCPCOUNTER, XCELL, and TIDE algorithms. As shown in Figure 8A, there was a positive correlation between RBM10 and CAFs in HNSC-HPV, KIRP, and TGCT (Fig. 8A). For KIRC, OV, SKCM, SKCM-Metastasis, TGCT, THCA, and uveal melanoma (UVM), a positive correlation was observed between RBM10 expression and the abundance of endothelial cells (Fig. 8B).

Enrichment analysis of RBM10 and co-expression genes in pan-cancer

The pathways enriched in RBM10-interacting proteins and co-expressed genes were also explored, and an integrated network of RBM10-binding proteins was constructed using STRING (Fig. 9A). The top 100 genes correlated with RBM10 expression were screened from TCGA datasets using the GEPIA2 tool. As shown in Figure 9B, RBM10 was positively associated with upstream binding transcription factor (UBTF), scaffold attachment factor B (SAFB), DEXH-Box protein (DHX30), heterogeneous nuclear ribonucleoprotein A0 (HNRNPA0) and SURP and G-patch domain containing 1 (SUGP1). Furthermore, the expression of RBM10 was strongly and positively correlated with that of these five genes in most cancer types (Fig. 9C).

GO and KEGG enrichment analyses of the co-expressed genes revealed that "humoral immune response", "DNA-binding transcription activator activity", "growth factor activity", "cell killing" and "chemical carcinogenesis" were the most enriched pathways, and these genes may, therefore, mediate the effect of RBM10 on tumorigenesis and development (Fig. 9D).

Discussion

The emergence of various analytical tools has made it possible for clinicians and cancer researchers to analyze disease-related genes in depth. In this study, we analyzed the pan-cancer genomic, transcriptomic, epigenetic, immunological, and prognostic data related to RBM10.

In recent years, the role of RBM10 in several diseases, including TARP syndrome and cancer, has been gradually unearthed (Imagawa et al., 2020; Zhang et al., 2020b; Xiao et al., 2021). RBM10 loss-of-function mutations are the cause of TARP syndrome, an abnormal developmental disorder that usually results in the death of the newborn (Johnston et al., 2010; Gripp et al., 2011). Furthermore, pre-clinical studies have shown that RBM10 has an inhibitory effect on the proliferation and clonogenicity of tumor cells *in vitro* and *in vivo*, and increases apoptosis rates (Jin et al., 2019; Jung et al., 2020a,b). On the other hand, more recent studies have suggested an oncogenic function of RBM10 (Loiselle et al., 2017; Rodor et al., 2017; Sun et al., 2019). This functional dichotomy highlights the importance of elucidating the molecular mechanisms underlying the effects of RBM10. Rodor et al. noted that RBM10 may have cell type and/or species-specific roles (Rodor et al., 2017), and very little is known regarding RBM10 splice variant interacting factors. Given that different isoforms may have opposing functions (Loiselle et al., 2017), the ratio of the various RBM10 isoforms in a patient could be of predictive significance for disease incidence and/or progression.

Understanding the mechanisms that regulate RBM10 expression and function would help to predict the impact of RBM10 on cellular processes and thus potential patient outcomes in a disease such as cancer. To this end, we analyzed *RBM10* gene expression in 33 different tumors based on TCGA data. RBM10 was upregulated in fifteen cancer types compared with the corresponding normal tissues. The difference in RBM10 expression levels across various cancers may reflect distinct functions and mechanisms. In addition, KIRP and LIHC patients with high tumor expression of RBM10 had poor overall survival. These results suggest that RBM10 is a potential prognostic biomarker of cancer.

Mutations are major drivers of tumor initiation and progression (Omholt et al., 2002, Mutvei et al., 2015; Pérez-Rivas et al., 2018; Ge et al., 2021). *RBM10* mutations have been reported in several cancer types, although little is known regarding the correlation between *RBM10* mutations and cancer prognosis (Ibrahimpasic et al., 2017, Zhao et al., 2017). We explored these potential correlations using the cBioPortal tool and found that genetic alterations in *RBM10* did not confer a survival benefit to BLCA, LUAD and LUSC patients. Recent evidence indicates that the tumor mutation burden (TMB) is a marker of the response to immune checkpoint blockade (Zhu et al., 2019). Several clinical trials have shown that high TMB is associated with enhanced objective response rates to PD-1/PD-L1 inhibitors compared with that in low TMB patients (Leslie, 2018; Samstein et al., 2019; Zhu et al., 2019). We found that RBM10 expression was positively correlated with that of PD-L1 in seven cancers, except for THCA and LUAD, and with that of CTLA4 in HNSC, STAD, LIHC, and LUAD. Furthermore, RBM10 expression was positively correlated with immune cell infiltration in six cancer types but not in HNSC, BRCA, THCA, and LUAD. Likewise, a positive correlation was observed between the expression of RBM10 and the abundance of stromal cells, including CAFs and endothelial cells. These findings altogether indicate that RBM10 plays an important role in the tumor microenvironment. Finally, GO and KEGG pathway analyses revealed that the genes co-expressed with RBM10 were mainly enriched in the "humoral immune response pathway". This is consistent with recent reports indicating a close association between the expression of RBM10 and immune activity (Liu et al., 2021b; Pozzi et al., 2020). RBM10 over-expression induces RIG-I

(retinoic acid-inducible gene I) ubiquitination, which triggers a robust innate immune response (Pozzi et al., 2020).

This study has several limitations that ought to be considered. First, our findings are based on data retrieved from different online databases, which may have caused heterogeneity. Therefore, the potential role of RBM10 in cancer will have to be validated in larger cohorts and through experimental and clinical studies. Moreover, the mechanisms will have to be elucidated in future studies to explain the discrepancy between our results and part of previous studies. Finally, it is difficult to predict and evaluate the efficacy of immunotherapy based only on expression data. Therefore, further *in vitro* and *in vivo* studies are warranted to affirm our results.

Conclusions

In summary, we comprehensively analyzed RBM10 in pan-cancer. We explored RBM10 expression, clinical prognosis, mutations, phosphorylation, immune infiltration, and potential function in a variety of human cancers. These findings help to clarify the role of RBM10 in tumorigenesis from a variety of perspectives and provide new insights into an anti-tumor immune strategy based on the expression of RBM10.

Acknowledgements. The authors thank all the researchers and staff who supported ONCOMINE, UALCAN, GEPIA2, Kaplan–Meier Plotter, cBioPortal, STRING, and TIMER.

Ethics approval and consent to participate. No ethical questions.

Consent for publication. Not applicable.

Availability of Data and Material. The datasets analyzed during the current study are available from TCGA (https://portal.gdc.cancer.gov/), GEPIA2 (http://gepia2.cancer-pku.cn/#analysis), CPTAC (https://proteomics.cancer.gov/data-portal), HPA (https://www.proteinatlas.org/), cBioPortal (http://www.cbioportal.org), String (http://string-db.org), KEGG (www.kegg.jp/kegg/kegg1.html), and TIMER (http://timer.cistrome.org/).

Competing interests. The authors declare that the research was conducted in the absence of any commercial or financial relationships that could be construed as a potential conflict of interest.

Funding. This study was supported by the Haiyan Foundation of Harbin Medical University Cancer Hospital (JJZD2020-14).

Author Contributions. XS, DXJ, and YY designed and planned the study concept. XS and DXJ analyzed data and drafted the manuscript. YY: Final review and authorization. All authors have read and agreed to the published version of the manuscript.

References

Bechara E.G., Sebestyen E., Bernardis I., Eyras E. and Valcárcel J. (2013). RBM5, 6, and 10 differentially regulate NUMB alternative splicing to control cancer cell proliferation. Mol. Cell. 52, 720-733.

Benci J.L., Xu B., Qiu Y., Wu T.J., Dada H., Victor C.T.-S., Cucolo L., Lee D.S.M., Pauken K.E., Huang A.C., Gangadhar T.C., Amaravadi R.K., Schuchter L.M., Feldman M.D., Ishwaran H., Vonderheide R.H., Maity A., Wherry E.J. and Minn A.J. (2016). Tumor interferon signaling regulates a multigenic resistance program to immune checkpoint blockade. Cell 167, 1540-1554.

Chen F., Chandrashekar D.S., Varambally S. and Creighton C.J. (2019). Pan-cancer molecular subtypes revealed by mass-spectrometry-based proteomic characterization of more than 500 human cancers. Nat. Commun. 10, 5679.

Chouaib S., Kieda C., Benlalam H., Noman M.Z., Mami-Chouaib F. and Rüegg C. (2010). Endothelial cells as key determinants of the tumor microenvironment: inter-action with tumor cells, extracellular matrix and immune killer cells. Crit. Rev. Immunol. 30, 529-545.

Cui X., Zhang X., Liu M. and Zhao C. (2020). A pan-cancer analysis of the oncogenic role of staphylococcal nuclease domain-containing protein 1 (SND1) in human tumors. Genomics 112, 3958-3967.

Gao J., Aksoy B.A., Dogrusoz U. Dresdner G., Gross B., Sumer S.O., Sun Y., Jacobsen A., Sinha R., Larsson E., Cerami E., Sander C. and Schultz N. (2013). Integrative analysis of complex cancer genomics and clinical profiles using the cBioPortal. Sci. Signal. 6, pl1.

Ge Z., Helmijr J.C.A., Jansen M.P.H.M., Boor P.P.C., Noordam L., Peppelenbosch M., Kwekkeboom J., Kraan J. and Sprengers D. (2021). Detection of oncogenic mutations in paired circulating tumor DNA and circulating tumor cells in patients with hepatocellular carcinoma. Transl. Oncol. 14, 101073.

Gripp K.W., Hopkins E., Johnston J.J., Krause C., Dobyns W.B. and Biesecker L.G. (2011). Long-term survival in TARP syndrome and confirmation of RBM10 as the disease-causing gene. Am. J. Med. Genet A. 155A, 2516-2520.

Ibrahimpasic T., Xu B., Landa I., Dogan S., Middha S., Seshan V., Deraje S., Carlson D.L., Migliacci J., Knauf J.A., Untch B., Berger M.F., Morris L., Tuttle R.M., Chan T., Fagin J.A., Ghossein R., and Ganly I., (2017). Genomic alterations in fatal forms of non-anaplastic thyroid cancer: Identification of *MED12* and *RBM10* as novel thyroid cancer genes associated with tumor virulence. Clin. Cancer Res. 23, 5970-5980.

Imagawa E., Konuma T., Cork E.E., Diaz G.A. and Oishi K. (2020). A novel missense variant in RBM10 can cause a mild form of TARP syndrome with developmental delay and dysmorphic features. Clin. Genet. 98, 606-612.

Inoue A., Yamamoto N., Kimura M., Nishio K., Yamane H. and Nakajima K. (2014). RBM10 regulates alternative splicing. FEBS Lett. 588, 942-947.

Jin X., Di X., Wang R., Ma H., Tian C., Zhao M., Cong S., Liu J., Li R. and Wang K. (2019). RBM10 inhibits cell proliferation of lung adenocarcinoma via RAP1/AKT/CREB signalling pathway. J. Cell. Mol. Med. 23, 3897-3904.

Johnston J.J., Teer J.K., Cherukuri P.F., Hansen N.F., Loftus S.K., NIH Intramural Sequencing Center (NISC), Chong K., Mullikin J.C. and Biesecker L.G. (2010). Massively parallel sequencing of exons on the X chromosome identifies RBM10 as the gene that causes a syndromic form of cleft palate. Am. J. Hum. Genet. 86, 743-748.

Jung J.H., Lee H., Zeng S.X. and Lu H. (2020a). RBM10, a new regulator of p53. Cells 9, 2107.

Jung J.H., Lee H., Cao B., Liao P., Zeng S.X. and Lu H. (2020b). RNA-binding motif protein 10 induces apoptosis and suppresses proliferation by activating p53. Oncogene 39, 1031-1040.

Kuang X.Y., Jiang H.S., Li K., Zheng Y.-Z., Liu Y.-R., Qiao F., Li S., Hu X. and Shao Z.M. (2016). The phosphorylation-specific association of STMN1 with GRP78 promotes breast cancer metastasis. Cancer Lett. 377, 87-96.

Leslie M. (2018). High TMB predicts immunotherapy benefit. Cancer Discov. 8, 668.

Liu X., Zhang Y., Wang Y., Yang M., Hong F. and Yang S. (2021a). Protein phosphorylation in cancer: Role of nitric oxide signaling pathway. Biomolecules 11, 1009.

Liu B., Wang Y., Wang H., Li Z., Yang L., Yan S., Yang X., Ma Y., Gao X., Guan Y., Yi X., Xia X., Li J. and Wu N. (2021b). RBM10 deficiency is associated with increased immune activity in lung adenocarcinoma. Front. Oncol. 11, 677826.

Loiselle J.J., Roy J.G. and Sutherland L.C. (2017). RBM10 promotes transformation-associated processes in small cell lung cancer and is directly regulated by RBM5. PLoS One 12, e0180258.

Mao X., Xu J., Wang W., Liang C., Hua J., Liu J., Zhang B., Meng Q., Yu X. and Shi S. (2021). Crosstalk between cancer-associated fibroblasts and immune cells in the tumor microenvironment: new findings and future perspectives. Mol. Cancer 20, 131.

Mueller C.F., Berger A., Zimmer S., Tiyerili V. and Nickening G. (2009). The heterogenous nuclear riboprotein S1-1 regulates AT1 receptor gene expression via transcriptional and posttranscriptional mechanisms. Arch. Biochem. Biophys. 488, 76-82.

Murciano-Goroff Y.R., Warner A.B. and Wolchok J.D. (2020). The future of cancer immunotherapy: microenvironment-targeting combinations. Cell Res. 30, 507-519.

Mushtaq A., Mir U.S. and Altaf M. (2023). Multifaceted functions of RNA-binding protein vigilin in gene silencing, genome stability, and autism-related disorders. J. Biol. Chem. 299, 102988.

Mutvei A.P., Fredlund E. and Lendahl U. (2015). Frequency and distribution of Notch mutations in tumor cell lines. BMC Cancer 15, 311.

Nagy Á., Lánczky A., Menyhárt O. and Győrffy B. (2018). Validation of miRNA prognostic power in hepatocellular carcinoma using expression data of independent datasets. Sci. Rep. 8, 9227.

Okholm T.L.H., Sathe S., Park S.S., Kamstrup A.B., Rasmussen A.M., Shankar A., Chua Z.M., Fristrup N., Nielsen M.M., Vang S., Dyrskjot L., Aigner S., Damgaard C.K., Yeo G.W. and Pedersen J.S. (2020). Transcriptome-wide profiles of circular RNA and RNA-binding protein in-teractions reveal effects on circular RNA biogenesis and cancer pathway expression. Genome Med. 12, 112.

Omholt K., Karsberg S., Platz A., Kanter L., Ringborg U. and Hansson J. (2002). Screening of N-ras codon 61 mutations in paired primary and metastatic cutaneous melanomas: mutations occur early and persist throughout tumor progression. Clin. Cancer Res. 8, 3468-3474.

Pang S.J., Sun Z., Lu W.-F., Si-Ma H., Lin Z.-P., Shi Y., Yang Y.-C., Zhao X.-J., Yang G.-S., Jin G.-Z. and Yang N. (2022). Integrated bioinformatics analysis and validation of the prognostic value of *RBM10* expression in hepatocellular carcinoma. Cancer Manag. Res. 14, 969-980.

Pérez-Rivas L.G., Theodoropoulou M., Puar T.H., Fazel J., Stieg M.R., Ferraù F., Assié G., Gadelha M.R., Deutschbein T., Fragoso M.C., Kusters B., Saeger W., Honegger J., Buchfelder M., Korbonits M., Bertherat J., Stalla G.K., Hermus A.R., Beuschlein F. and Reincke M. (2018). Somatic *USP8* mutations are frequent events in corticotroph tumor progression causing Nelson's tumor. Eur. J. Endocrinol. 178, 57-63.

Pozzi B., Bragado L., Mammi P., Torti M.F., Gaioli N., Gebhard L.G., Solá M.E.G., Vaz-Drago R., Iglesias N.G., García C.C., Gamarnik A.V. and Srebrow A. (2020). Dengue virus targets RBM10 deregulating host cell splicing and innate immune response. Nucleic Acids Res. 48, 6824-6838.

Rhodes D.R., Yu J., Shanker K., Deshpande N., Varambally R., Ghosh D., Barrette T., Pandey A., Chinnaiyan A.M. (2004). ONCOMINE: a cancer microarray database and integrated data-mining platform. Neoplasia 6, 1-6.

Rodor J., FitzPatrick D.R., Eyras E. and Caceres J.F. (2017). The RNA-binding landscape of RBM10 and its role in alternative splicing regulation in models of mouse early development. RNA Biol. 14, 45-57.

Samstein R.M., Lee C.H., Shoushtari A.N., Hellmann M.D., Shen R., Janjigian Y.Y., Barron D.A., Zehir A., Jordan E.J., Omuro A., Kaley T.J., Kendall S.M., Motzer R.J., Hakimi A.A., Voss M.H., Russo P., Rosenberg J., Iyer G., Bochner B.H., Bajorin D.F., Al-Ahmadie H.A., Chaft J.E., Rudin C.M., Riely G.J., Baxi S., Ho A.L., Wong R.J., Pfister D.G., Wolchok J.D., Barker C.A., Gutin P.H., Brennan C.W., Tabar V., Mellinghoff I.K., DeAngelis L.M., Ariyan C.E., Lee N., Tap W.D., Gounder M.M., D'Angelo S.P., Saltz L., Stadler Z.K., Scher H.I., Baselga J., Razavi P., Klebanoff C.A., Yaeger R., Segal N.H., Ku G.Y., DeMatteo R.P., Ladanyi M., Rizvi N.A., Berger M.F., Riaz N., Solit D.B., Chan T.A. and Morris L.G.T. (2019). Tumor mutational load predicts survival after immunotherapy across multiple cancer types. Nat. Genet. 51, 202-206.

Sturm G., Finotello F., Petitprez F., Zhang J.D., Baumbach J., Fridman W.H., List M. and Aneichyk T. (2019). Comprehensive evaluation of transcriptome-based cell-type quantification methods for immuno-oncology. Bioinformatics 35, i436-i445.

Soongsathitanon J., Jamjuntra P., Sumransub N., Yangngam S., De la Fuente M., Landskron G., Thuwajit P., Hermoso M.A. and Thuwajit C. (2021). Crosstalk between Tumor-Infiltrating immune cells and cancer-associated fibroblasts in tumor growth and immunosuppression of breast cancer. J. Immunol. Res. 2021, 8840066.

Sun X., Jia M., Sun W., Feng L., Gu C. and Wu T. (2019). Functional role of RBM10 in lung adenocarcinoma proliferation. Int. J. Oncol. 54, 467-478.

Wang Y., Gogol-Doring A., Hu H., Frohler S., Ma Y., Jens M., Maaskola J., Murakawa Y., Quedenau C., Landthaler M., Kalscheuer V., Wieczorek D., Wang Y., Hu Y. and Chen W. (2013). Integrative analysis revealed the molecular mechanism underlying RBM10-mediated splicing regulation. EMBO Mol. Med. 5, 1431-1442.

Wu J., Liu G., An K. and Shi L. (2022). NPTX1 inhibits pancreatic cancer cell proliferation and migration and enhances chemotherapy sensitivity by targeting RBM10. Oncol. Lett. 23, 154.

Xiao S.J., Wang L.Y., Kimura M., Kojima H., Kunimoto H., Nishiumi F., Yamamoto N., Nishio K., Fujimoto S., Kato T., Kitagawa S., Yamane H., Nakajima K. and Inoue A. (2013). S1-1/RBM10: multiplicity and cooperativity of nuclear localisation domains. Biol. Cell. 105, 162-174.

Xiao W., Chen X., Li X., Deng K., Liu H., Ma J., Wang Z., Hu Y. and Hou J. (2021). RBM10 regulates human TERT gene splicing and inhibits pancreatic cancer progression. Am. J. Cancer Res. 11, 157-170.

Xing Y., Ruan G., Ni H., Qin H., Chen S., Gu X., Shang J., Zhou Y., Tao X. and Zheng L. (2021). Tumor immune microenvironment and its related miRNAs in tumor progression. Front. Immunol. 12, 624725.

Yin S., Chen Y., Chen Y., Xiong L. and Xie K. (2023). Genome-wide profiling of rice Double-stranded RNA-Binding protein 1-associated RNAs by targeted RNA editing. Plant Physiol. 192, 805-820.

Yu G., Wang L.G., Han Y. and He Q.Y. (2012). clusterProfiler: an R package for comparing biological themes among gene clusters. OMICS 16, 284-287.

Yuan Z., Cui H., Wang S., Liang W., Cao B., Song L., Liu G., Huang J., Chen L. and Wei B. (2023). Combining neoadjuvant chemotherapy with PD-1/PD-L1 inhibitors for locally advanced, resectable gastric or gastroesophageal junction adenocarcinoma: A systematic review and meta-analysis. Front. Oncol. 13, 1103320.

Zhang S., Zeng Z., Liu Y., Huang J., Long J., Wang Y., Peng X., Hu Z. and Ouyang Y. (2020a). Prognostic landscape of tumor-infiltrating immune cells and immune-related genes in the tumor microenvironment of gastric cancer. Aging 12, 17958-17975.

Zhang S., Bao Y., Shen X., Pan Y., Sun Y., Xiao M., Chen K., Wei H., Zuo J., Saffen D., Zong W.-X., Sun Y., Wang Z. and Wang Y. (2020b). RNA binding motif protein 10 suppresses lung cancer progression by controlling alternative splicing of eukaryotic translation initiation factor 4H. EBioMedicine 61, 103067.

Zhang J., Zhang J., Wang F., Xu X., Li X., Guan W., Men T. and Xu G. (2021). Overexpressed COL5A1 is correlated with tumor progression, paclitaxel resistance, and tumor-infiltrating immune cells in ovarian cancer. J. Cell. Physiol. 236, 6907-6919.

Zhao J., Sun Y., Huang Y., Song F., Huang Z., Bao Y., Zuo J., Saffen D., Shao Z., Liu W. and Wang Y. (2017). Functional analysis reveals that RBM10 mutations contribute to lung adenocarcinoma pathogenesis by deregulating splicing. Sci. Rep. 7, 40488.

Zhao C., Tao T., Yang L., Qin Q., Wang Y., Liu H., Song R., Yang X., Wang Q., Gu S., Xiong Y., Zhao D., Wang S., Feng D., Jiang W.G., Zhang J. and He J. (2019). Loss of PDZK1 expression activates PI3K/AKT signaling via PTEN phosphorylation in gastric cancer. Cancer Lett. 453, 107-121.

Zheng S., Damoiseaux R., Chen L. and Black D.L. (2013). A broadly applicable high-throughput screening strategy identifies new regulators of Dlg4 (Psd-95) alternative splicing. Genome Res. 23, 998-1007.

Zheng L., Xiong A., Wang S., Xu J., Shen Y., Zhong R., Lu J., Chu T., Zhang W., Li Y., Zheng X., Han B., Zhong H., Nie W. and Zhang X. (2023). Decreased monocyte-to-lymphocyte ratio was associated with satisfied outcomes of first-line PD-1 inhibitors plus chemotherapy in stage IIIB-IV non-small cell lung cancer. Front. Immunol. 14, 1094378.

Zhu J., Zhang T., Li J., Lin J., Liang W., Huang W., Wan N. and Jiang J. (2019). Association between Tumor Mutation Burden (TMB) and outcomes of cancer patients treated with PD-1/PD-L1 inhibitions: A meta-analysis. Front. Pharmacol. 10, 673.

Zhu C., Xue J., Wang Y., Wang S., Zhang N., Wang Y., Zhang L., Yang X., Long J., Yang X., Sang X. and Zhao H. (2023). Efficacy and safety of lenvatinib combined with PD-1/PD-L1 inhibitors plus Gemox chemotherapy in advanced biliary tract cancer. Front. Immunol. 14, 1109292.

Accepted July 4, 2024